Friction

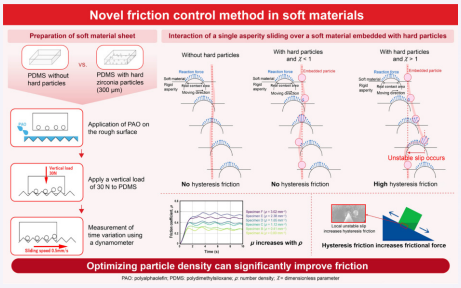
Research Article

Friction control in soft materials enabled through local stick–slip motion at contact interface

Kazushi Ito[1], Satoru Maegawa[1,✉], Izumi Yoshida[1], Xiaoxu Liu[1], Fumihiro Itoigawa[1], Naoya Amino[2]

Cite this article: Ito K, Maegawa S, Yoshida I, et al. *Friction* 2026, **14**(3): 9441167. https://doi.org/10.26599/FRICT.2025.9441167

ABSTRACT: This paper presents a novel friction control method that introduces internal stiffness inhomogeneity into soft material surfaces that slide on rough surfaces. This approach involves embedding hard particles within a soft material to control friction. When these particles encounter asperities on a rough surface during sliding, they trigger a local stick–slip-like motion that leads to energy dissipation and increased macroscopic friction. The validity of the concept was demonstrated through experiments using a simplified setup with triangular periodic one-dimensional roughness. This method is expected to be useful for designing various soft material sliding surfaces.



KEYWORDS: friction control; stiffness inhomogeneity; soft materials; stick–slip

1 Introduction

Owing to their unique elastic properties, soft materials such as rubber and elastomers are widely used in various tribological applications, including shoe soles [1, 2], automotive tires [3], industrial grippers [4], and mechanical seals [5]. In these applications, controlling frictional forces is essential for ensuring safety, enhancing durability, and optimizing performance.

Various approaches to friction control have been proposed based on the deformable nature of soft materials. Research on surface texture design and implementation is a prime example. These designs aim to enhance frictional performance by optimizing the interaction between the soft material and its counterface, often leveraging the inherent compliance of the material to increase the real contact area, manage lubricant distribution, or induce desirable deformation patterns during sliding [6–11]. Texturing also controls the stress distribution across a rubber contact surface comprising multiple contact points, thereby accelerating the onset of sliding at each contact point. This can reduce the macroscopic static friction force and suppress the occurrence of stick–slip motion [9, 12–14]. Recently, other methods have been proposed to control the friction anisotropy for asymmetrically structured bioinspired surfaces and asperity height distribution design to obtain the desired friction law [15, 16]. Additionally, it is known that a surface texture design that leverages the characteristics of soft matter is crucial not only for addressing frictional forces but also for tackling adhesive forces [17, 18].

Research on internal inhomogeneity, similar to studies focusing on surface inhomogeneity, such as texturing, has also been conducted. By embedding fine particles or fibrous materials into the substrate of a soft material interface, stiffness inhomogeneity is created, which can increase the local contact stress by interlocking with the opposing surface or enhancing friction under mixed or fluid lubrication owing to the squeeze motion [19, 20]. An example of internal inhomogeneity is the control of friction and adhesion by inducing interfacial buckling through the application of a textile-embedded elastomer surface [21]. Additionally, numerical simulations have been conducted to explore the relationship between local behavior and the macroscopic friction coefficient when surface and internal inhomogeneities occur simultaneously [22].

Rubber friction is generally expressed as the sum of the adhesive and hysteresis components [23]. The former refers to the frictional force caused by intermolecular forces at the interface [24], whereas the latter is due to the energy dissipation that occurs when the rubber periodically deforms due to the multiple asperities of the mating surface [25]. Friction force is generated due to the asymmetry in contact stress and contact area before and after the rubber comes into contact with each asperity. Therefore, tanδ, which indicates the magnitude of energy dissipation, has been used as a design parameter for rubber friction. In addition to these adhesion and hysteresis frictions, the friction control methods focusing on the surface and internal inhomogeneities described above utilize geometric effects [26] based on engagement with the mating surface. If this geometrical factor is successfully utilized, it is expected that a new approach to friction control, distinct from the conventional tanδ-based design,

[1] Department of Electrical and Mechanical Engineering, Nagoya Institute of Technology, Gokiso-cho Showa-ku, Nagoya-shi, Aichi 466-8555, Japan. [2] The Yokohama Rubber Company, Ltd., 2-1 Oiwaki, Hiratsuka-shi, Kanagawa 254-8601, Japan.

✉ Corresponding author. E-mail: maegawa.satoru@nitech.ac.jp

Received: December 29, 2024; Revised: July 19, 2025; Accepted: August 13, 2025

© The Author(s) 2026. This is an open access article under the terms of the Creative Commons Attribution 4.0 International License (CC BY 4.0, http://creativecommons.org/licenses/by/4.0/).

can be established. For example, as discussed later in this paper, the ability to increase the friction coefficient depending on the number density of embedded hard particles is considered as one such example.

Based on the above background, this study presents an example of a friction control method based on the introduction of internal stiffness inhomogeneity in the friction between a rough surface and a soft material. Figure 1 presents an overview of the friction control approach used in this study. This study examined friction control using soft material sheets embedded with hard particles, focusing on the interlocking effect between the embedded particles and asperities on rough surfaces. When these particles encounter asperities on a rough surface during sliding, they trigger a local stick–slip-like motion that leads to energy dissipation and increased macroscopic friction. The validity of the concept was demonstrated through experiments using a simplified setup with triangular periodic one-dimensional roughness. This method is expected to be useful for designing various soft material sliding surfaces.

2 Concept of this study

The friction enhancement effect proposed in this study is explained using Figs. 2–4. Figure 2 shows a snapshot of a single asperity with opposing surface roughness sliding over a soft material sheet with embedded hard particles. The soft material sheet was fixed while the asperity moved from left to right at a constant speed. The blue vectors in the figure represent the contact reaction pressure distribution acting on the surface of the soft material sheet, whereas the red circles represent the embedded hard particles. To illustrate the essence of our friction control method, it was assumed that no adhesive friction force was generated at the contact surface.

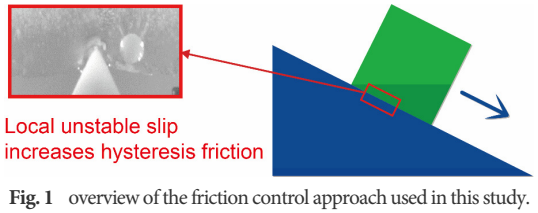


Fig. 1 overview of the friction control approach used in this study.

Figure 2(a) shows asperity sliding during contact with a homogeneous soft material sheet without embedded hard particles. Because it is a uniform elastic field, the same contact stress distribution always moves from left to right with a change in the asperity position. The red band in the figure represents the time variation of the horizontal displacement at any arbitrary point. As the asperity approaches, the material deforms because of the rightward contact reaction force. However, when the asperity exceeds the peak, the displacement returns to the origin in the horizontal direction. After the asperity passed, the material deformed to the left and eventually returned to its original position.

Figures 2(b) and 2(c) focus on the cases in which hard particles are embedded. In this case, unlike in Fig. 2(a), the internal stiffness becomes nonuniform owing to the presence of hard particles inside [27]. Consequently, the contact reaction force is not symmetric, and its magnitude varies depending on the positional relationship between the hard particles and the asperity. The difference between Figs. 2(b) and 2(c) illustrates whether elastic instability occurs when hard particles overcome asperity.

The Prandtl–Tomlinson model [28] is typically useful for modeling microscopic phenomena at the atomic scale; however, it is also helpful for visualizing the differences between Figs. 2(b) and 2(c). A simplified Prandtl–Tomlinson model is shown in Fig. 3. The mass point was fixed using a spring with stiffness k. The opposite end of the spring moves to the right at velocity V, and the interaction with the lower surface of the object is replaced by a periodic potential. Compared with Fig. 2, the mass point corresponds to the hard particle embedded in the soft material sheet, the spring corresponds to the effective stiffness of the soft material supporting the hard particle, and the periodic potential corresponds to the potential arising from the contact reaction force caused by the roughness of the counterpart surface. In the experimental setup, asperity is driven. However, in Fig. 3, to correspond to the general Prandtl–Tomlinson model, it is assumed that the mass point moves to the right. The equation of motion in this case is shown in Eq. (1):

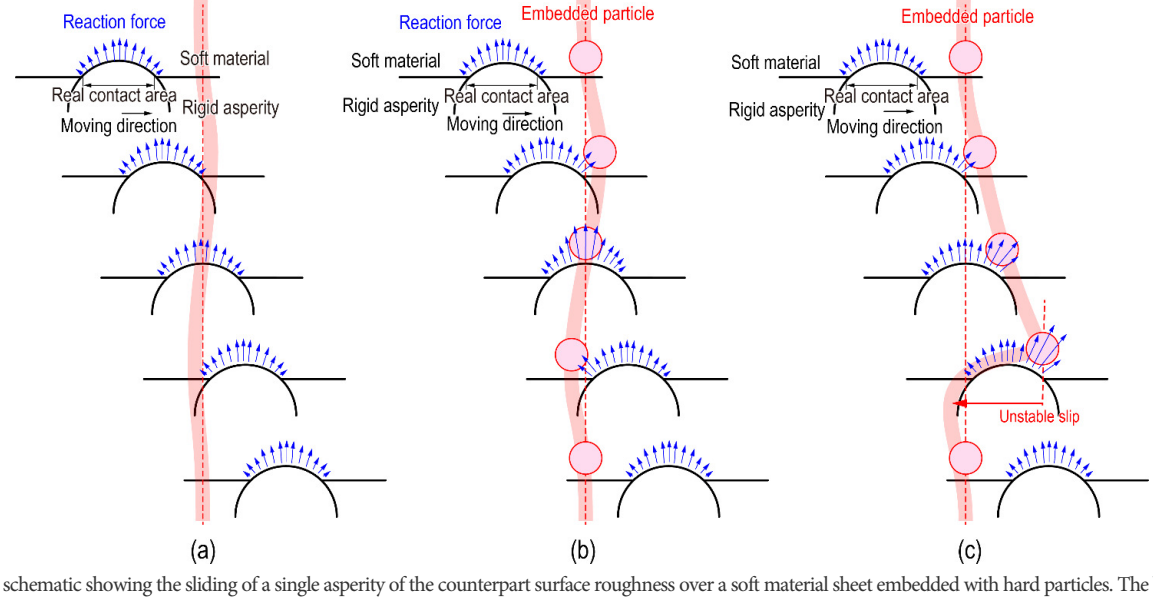


Fig. 2 A schematic showing the sliding of a single asperity of the counterpart surface roughness over a soft material sheet embedded with hard particles. The blue vector represents the contact reaction force, the red circles represent the hard particles, and the red bands indicate the path of the time variation of the lateral displacement. (a) A homogeneous rigid material without hard particles, (b) a case where hard particles are embedded, and the instability parameter χ of the Tomlinson model, discussed later, is less than 1, and (c) a case where hard particles are embedded and χ is greater than 1.

$$m\frac{\mathrm{d}^2x}{\mathrm{d}t^2} = -\gamma\frac{\mathrm{d}x}{\mathrm{d}t} - k(x_\mathrm{g} - x) - \frac{\mathrm{d}U(x)}{\mathrm{d}x} \quad (1)$$

where m is the effective mass of the mass point, γ is a constant representing the magnitude of energy dissipation proportional to velocity, k is the spring stiffness, x is the position of the mass point, x_g is the position of the spring's end, and U is the periodic potential defined as Eq. (2):

$$U(x) = -U_0\cos\left(\frac{2\pi}{a}x\right) \quad (2)$$

where U_0 and a are the amplitude and pitch of periodic potential.

To understand the essence of the phenomenon, let us consider the case where the mass moves sufficiently slowly so that it can be treated quasi-statically. In this case, the dissipation term $(-\gamma\frac{\mathrm{d}x}{\mathrm{d}t})$ can be neglected, and the time-averaged force of the spring $k(x_\mathrm{g} - x)$, which oscillates with time, can be expressed as the kinetic friction force.

It is well known that a system in the Prandtl–Tomlinson model exhibits elastic instability [29]. By introducing the dimensionless parameter $\chi = (2\pi a)^2U_0/k$, under the condition $\chi < 1$, the mass point is driven stably along the periodic potential. On the other hand, under the condition $\chi > 1$, regions where the mass point cannot exist stably arise, leading to jumps during sliding.

Figure 4 shows the position dependence of the friction force for $\chi = 0.5$ and $\chi = 4$. The vertical axis in the figure represents the dimensionless friction force, where $\xi = x/(2\pi a)$ denotes the dimensionless position of the mass, and $\xi_\mathrm{g} = x_\mathrm{g}/(2\pi a)$ denotes the dimensionless position of the opposite end of the spring. In the case of $\chi = 0.5$, the dimensionless friction force fluctuates when overcoming the potential, but its time average becomes zero. In other words, the net friction force was zero. On the other hand, in the case of $\chi = 4$, it can be observed that a sawtooth-like stick–slip motion occurs. In this case, the time average was not zero, and a net friction force was generated.

In summary, when a soft material sheet with embedded hard particles slides over rough surface under low χ conditions, elastic instability does not occur, as shown in Fig. 2(b). In this case, no net frictional force is generated. However, as shown in Fig. 2(c), when elastic instability causes a local stick–slip at the contact surface under an enough highly χ conditions, a net frictional force is generated.

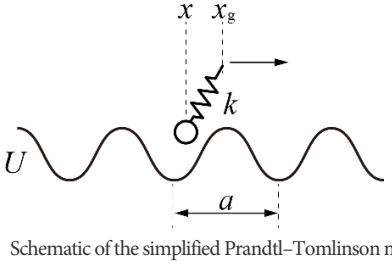


Fig. 3 Schematic of the simplified Prandtl–Tomlinson model.

In this model, the cause of stick–slip on the surface is considered to be the interlocking effect between the opposing surface roughness and hard particles. In other words, the focus is on the stick–slip phenomenon based on the stiffness inhomogeneity within the contact surface. However, the mechanisms that lead to stick–slip in soft materials can vary, including the propagation of Schallamach waves [30, 31] or the occurrence of abrasion wear [32]. Even in such cases, if local stick–slip occurs on the surface, an increase in frictional force can still be expected [33]. In the context of soft materials that easily deform and are prone to stick–slip, it is conceivable that friction control methods that leverage the occurrence of stick–slip could be effectively utilized.

Based on the above considerations, this study aims to explore the possibility of friction control through the induction of elastic instability, specifically local stick–slip, on the scale of the roughness of actual sliding surfaces. Specifically, by embedding hard particles and introducing stiffness inhomogeneity on the surface of a soft material, local stick–slip is generated. The effectiveness of this method is experimentally examined by comparing the amplitude of the vibrations caused by stick–slip with the increase in the friction force. Specifically, we conducted a sliding friction test between a soft material sheet with hard particles embedded on its surface and a periodically roughened surface. We measured the friction force and motion of the particles (local stick behavior) to quantify the effect of elastic instability on friction force improvement.

3 Experimental details and results

3.1 Experimental setup

Figure 5 shows a schematic of the experimental setup. As shown on the left side of the figure, a soft material sheet composed of polydimethylsiloxane (PDMS) with embedded hard particles was fixed to the top surface of the apparatus. The asperity on the opposing surface moves to the right. The top right of the figure shows an optical microscope image of the transparent PDMS sheet with hard particles embedded near the surface; the white dots represent zirconia particles with a diameter of 300 μm. The opposing surface was fixed on an x-direction automated stage and a z-direction motorized stage mounted on a dynamometer. The schematic in the lower-right side of the figure represents the roughness of the opposing surface. To simplify the phenomenon, a model roughness with a height of 0.5 mm, pitch of 1.0 mm, and apex angle of 90° was used. Surface roughness aligned vertically to the sliding direction. The positions of the hard particles during sliding were captured using a CCD camera installed at the top of the apparatus. Figure 6 shows a photograph of the apparatus.

The experimental procedure was as follows. To minimize the influence of adhesive friction and clearly highlight the friction enhancement effect due to the embedded hard particles, a

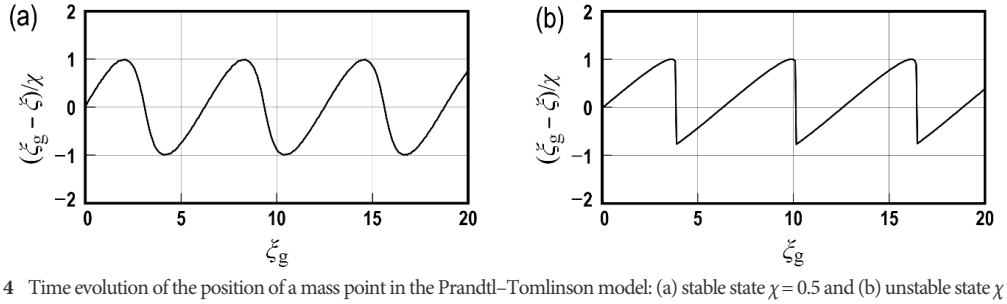


Fig. 4 Time evolution of the position of a mass point in the Prandtl–Tomlinson model: (a) stable state $\chi = 0.5$ and (b) unstable state $\chi = 4$.

清華大学出版社 Tsinghua University Press | SciOpen

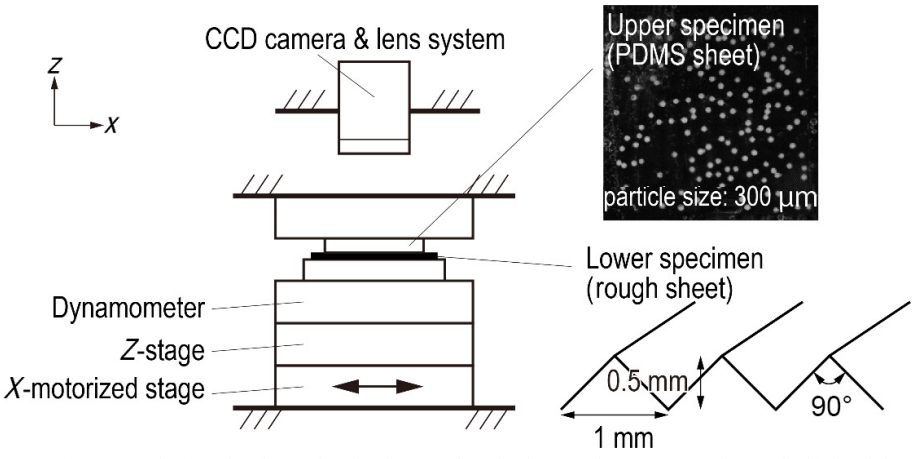


Fig. 5 Schematic of experimental apparatus developed in this study. The photograph in the diagram shows a PDMS sheet embedded with hard particles, and the inset at bottom right shows a schematic of the roughness profile of the mating surface.

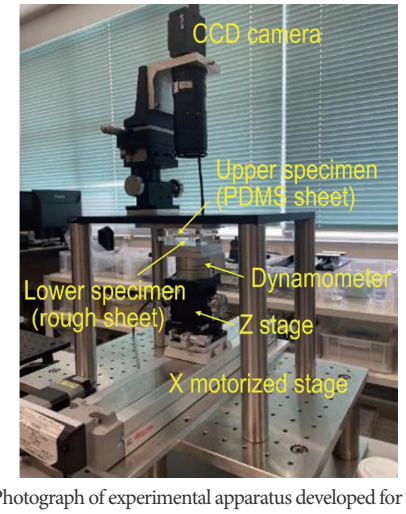


Fig. 6 Photograph of experimental apparatus developed for this study.

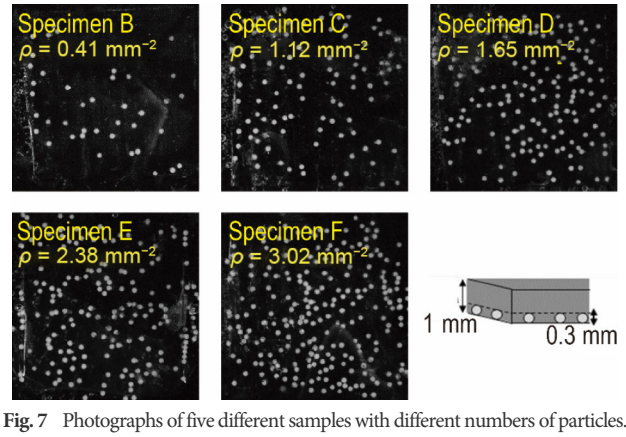


Fig. 7 Photographs of five different samples with different numbers of particles.

sufficient amount of polyalphaolefin (PAO; kinematic viscosity: 4 mm²/s@40 °C) was applied to the model rough surface of the opposing side. Subsequently, the rough surface of the model was pressed against a PDMS sheet using an automated z-direction stage. The contact reaction force (vertical load) was set as 30 N, and the x-direction automated stage was driven at a speed of 0.5 mm/s. The time variations in the vertical load and frictional force were measured using a dynamometer installed below the rough surface of the model. All experiments were conducted in a climate-controlled environment, with the temperature and relative humidity maintained at approximately 20–28 °C and 40%–60%, respectively.

3.2 Specimen

Based on the concept illustrated in Fig. 2, the friction enhancement effect is expected to increase as the number of hard particles increases.

Therefore, in this study, in addition to a reference specimen without hard particles, five specimens with different hard particle number densities were prepared, as shown in Fig. 7. The sample without hard particles was named Sample A, and as the number density of hard particles increased, the samples were named Sample B through Sample F. The number density of zirconia particles in each sample is indicated in Fig. 7. The specimens were prepared as follows: First, the PDMS base material and curing agent were mixed at a ratio of 10 : 1 and poured into a mold to form a sheet with a thickness of 0.7 mm. After the PDMS solidified, the sheet was removed from the mold, and zirconia particles with a diameter of 300 μm were randomly sprinkled onto the upper surface of the sheet. Subsequently, as shown in the schematic at the bottom right of Fig. 7, PDMS was poured into the gap of a 1 mm-thick mold and cured again to achieve a final thickness of 1 mm. The PDMS sheet was formed into a square shape with 10 mm sides and a thickness of 1 mm. The Young's modulus of the PDMS was 0.5 MPa. As shown in Fig. 7, the zirconia particles are randomly distributed near the surface on one side of the PDMS sheet. In the experiment, the lower face of schematic at the bottom right of Fig. 7 was used as the friction surface. This allows the interlocking effect to occur easily between the asperities of the counter surface and the zirconia particles within the PDMS sheet.

3.3 Experimental results

Figure 8 shows temporal variation of the friction coefficient μ, which is defined as $\mu = F_x/F_z$ using the vertical load F_z and the frictional force F_x measured by the dynamometer. It is evident from the figure that the average value of the friction coefficient increases with an increase in the number density of hard particles. This implies that the friction force can be controlled by changing the number of zirconia particles embedded in the PDMS sheet. Additionally, all the specimens exhibited a gentle oscillation with a period of 2 s. As shown in Fig. 8, the pitch of the opposing surface roughness was 1 mm and the driving speed was 0.5 mm/s. Accordingly, a new asperity entered the leading edge of the specimen every 2 s. It is predicted that the catching asperities at the edge of the specimen cause this fluctuation in the friction

coefficient. If the size of the specimen is increased, this edge effect is expected to be reduced, leading to smaller fluctuations in the friction coefficient.

Figure 9 shows the number density of hard particles on the horizontal axis, and the time-averaged friction coefficient in the steady state on the vertical axis. The overall trend indicates that the average friction coefficient increases with an increase in the number density of hard particles. However, a closer look reveals that under the condition with the highest number density, the friction coefficient does not increase but rather decreases. The friction coefficient in the absence of hard particles is approximately 0.3. This was assumed to be caused by the hysteresis friction component arising from the viscoelastic effect of the PDMS matrix, assuming that the adhesive friction force was sufficiently small owing to the application of the lubricant. Although PDMS is generally considered to exhibit near-elastic characteristics, the counter surface in this experiment had a very sharp apex angle of 90°, which likely led to significant hysteresis friction [26]. Additionally, it is possible that direct contact occurred because of oil film breakdown caused by localized increase in the contact pressure within the contact area. However, when a similar experiment was conducted with the surface roughness aligned parallel to the sliding direction, the frictional force was significantly reduced, suggesting that the former (hysteresis friction) is the primary cause.

4 Discussion

Based on the experimental results, we discuss the frictional force increase effect in soft elastomers by embedding hard particles.

Figure 10 shows an example of the measurement of the change in the position of particles in the sliding direction for Sample B, with four representative particle positions. Sample B was chosen for two reasons: it showed a friction increase with particle density, suggesting particle contribution to friction; and its low particle density meant that particle motion was less hindered by neighboring particles, allowing clearer observation of their behavior. The vertical axis in Fig. 10 shows the time variation of the particle position in the sliding direction, with the values adjusted so that the time-averaged position is set to zero. In all cases, there was a sharp change in position every 2 s as the asperities on the opposing surface passed (indicated by the downward arrows in the figure). This corresponds to elastic instability, that is, local stick–slip, as shown in Fig. 2(c). The opposing surface used in this experiment had a very acute angle of 90° at the apex, which was expected to result in a strong interlocking effect between the hard particles and the surface roughness. Based on the experimental results, we discuss the frictional force increase effect in soft elastomers by embedding hard particles. Additionally, an increase in the Young's modulus directly leads to an increase in the support stiffness, suppressing the occurrence of elastic instability. In other words, the increase in friction force owing to energy dissipation associated with elastic instability can be considered a method unique to soft materials.

To quantitatively estimate the amount of energy dissipation associated with the occurrence of local stick–slip, the average value of the displacement variation in the sliding direction of all the hard particles in each sample was calculated.

The results are shown in Fig. 11, where the vertical axis represents the difference between the minimum and maximum position variation (peak-to-peak amplitude), i.e., a_{p-p}, and the horizontal axis represents the number density of hard particles. To

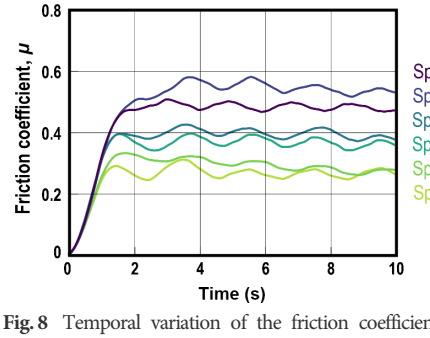


Fig. 8 Temporal variation of the friction coefficient μ for various number density of zirconia particles. Each data point is based on a single measurement conducted under the same procedure for each condition.

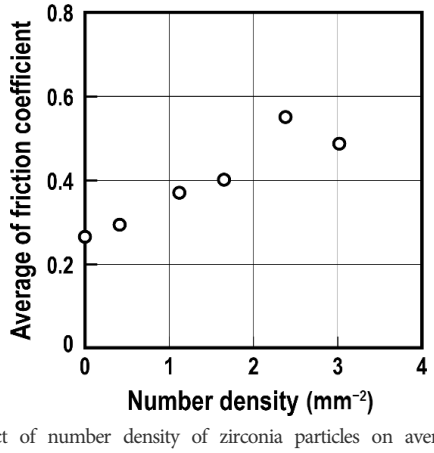


Fig. 9 Effect of number density of zirconia particles on average friction coefficient.

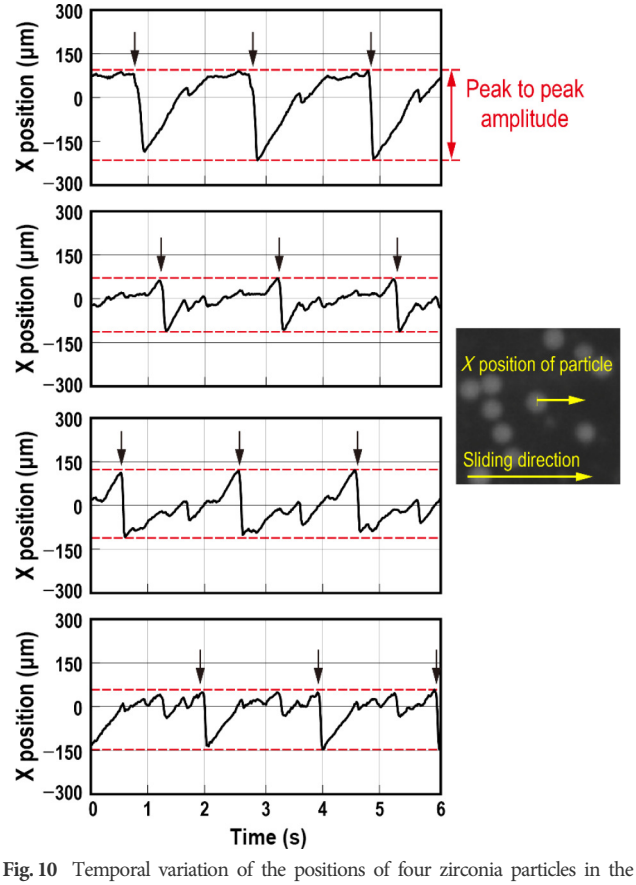


Fig. 10 Temporal variation of the positions of four zirconia particles in the sliding direction under sliding friction test for Sample B (particle density: 0.41 mm^{-2}).

清華大学出版社 Tsinghua University Press | SciOpen

calculate a_{p-p}, we determined the maximum amplitude of the time-dependent displacement of each particle in the specimen, as indicated by the red dashed lines in Fig. 10, and defined the average value over all particles as a_{p-p}. As shown in Fig. 11, it can be seen that a_{p-p} is almost constant regardless of the particle density. However, a closer look reveals that the mean amplitude is smaller under conditions of maximum number density. This is expected because, as the particle density increases, the distance between particles becomes shorter, making it more difficult for each particle to move independently. This is considered to result in an effective increase in the support stiffness of the particles. Consequently, elastic instabilities are either suppressed or, if they occur, their amplitudes become smaller, leading to a reduced frictional contribution from each particle due to local stick–slip. These mechanisms are thought to explain the observed decrease in the friction coefficient in the specimen with the highest particle density. Let ΔW_{single_ss} be the work done by the mass point during one local stick–slip event, then ΔW_{single_ss} is expressed using the tangential force p applied to the mass point supported by a spring with stiffness k and the displacement u as in Eq. (3):

$$\Delta W_{single_ss} = \int p\mathrm{d}u = \int ku\mathrm{d}u \tag{3}$$

where the integral range corresponds to the duration of one stick–slip event. Assuming that the waveform of the local stick–slip is approximately sawtooth-shaped, as shown in Fig. 3(b), the work performed by the mass point during one stick–slip event can be rewritten as in Eq. (4):

$$\Delta W_{single_ss} = \frac{1}{2} k a_{p-p}{}^2 \tag{4}$$

As shown in Fig. 10, it should be noted that each local stick–slip is not necessarily a perfect sawtooth shape, and the above approximation includes some errors. Assuming that all the work performed by the particle during the local stick–slip is dissipated, the frictional force induced by the local stick–slip motion $F_{stick-slip}$ is expressed by Eq. (5):

$$F_{stick-slip} = \frac{N\Delta W_{single\ stick-slip}}{\Delta l} = \frac{1}{2}\frac{Nka_{p-p}^2}{\Delta l} \tag{5}$$

where N is the total number of hard particles and Δl is the surface roughness pitch. The support stiffness of the particles, k was assumed to be identical for all specimens and was estimated to be 1,400 N/m through FEM simulations conducted using COMSOL Multiphysics. The values of a_{p-p} represent the average peak-to-peak amplitude for each specimen, as shown in Fig. 11.

Figure 12 shows the results of quantifying the proportion of the increase in frictional force owing to the occurrence of local stick–slip relative to the total frictional force. Here, $F_{original}$ represents the frictional force measured when a non-particle sample (Sample A) is used, and $F_{stick-slip}$ is the friction increase estimated using Eq. (4). In addition, F_{other} represents the portion of the increased frictional force caused by effects other than the work done by the local stick–slip. For example, embedding particles may lead to an increase in the local contact stress at the true contact areas, which can result in an increase in boundary friction [19]. F_{other} shows a similar trend to $F_{stick-slip}$, increasing from Sample A to E and then decreasing from E to F. One possible explanation is that as particle density increases, interlocking between the particles and the asperity enhances boundary friction, whereas at the highest particle density (E to F), interlocking becomes less likely, resulting in little change in contact area or contact pressure, and a subsequent decrease in F_{other}. In other words, this indicates that boundary friction may vary with particle embedding. Furthermore, not only adhesive and boundary friction but also hysteresis friction that does not originate from local stick–slip may be influenced. It should be noted that in Fig. 12, F_{other} is calculated based on the assumptions that changes in contact pressure and contact area due to particle embedding are negligible, and that $F_{original}$ remains constant. Accordingly, further investigation is required to verify the accuracy of this calculation. In any case, the increase in friction force caused by actively inducing localized stick–slip through the implantation of hard particles was demonstrated to have a useful effect on friction control. For example, in Samples E and F, the increase in friction force was more than 50% compared to the reference sample without embedded particles. As mentioned above, this friction increase effect is expected to decrease with increasing Young's modulus, and is a friction control technique unique to soft materials. From Eq. (5), it appears that $F_{stick-slip}$ increases with an increase in stiffness k, but because a_{p-p} decreases as k increases, $F_{stick-slip}$ decreases as k increases.

The abovementioned excitation of local elastic instability (local stick–slip) is expected to sufficiently increase the frictional force, and the experimental results show that this is the case. As mentioned earlier, using the Tomlinson model to interpret elastic instability, one would expect this frictional force increasing effect to decrease with, for example, a decrease in the mating-surface roughness or an increase in stiffness. This frictional force-increasing effect is only observed for soft materials that have low stiffness and are easily deformed.

In this study, we propose a friction control method that

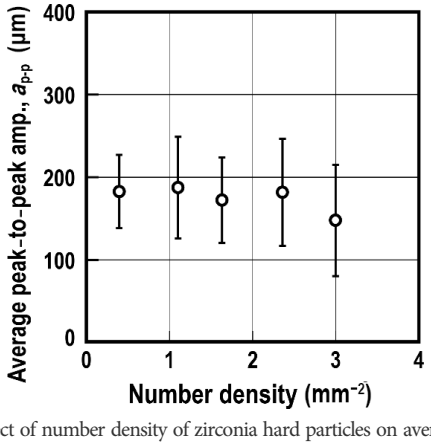


Fig. 11 Effect of number density of zirconia hard particles on average value of peak-to-peak amplitude a_{p-p}. Error bars represent standard deviation.

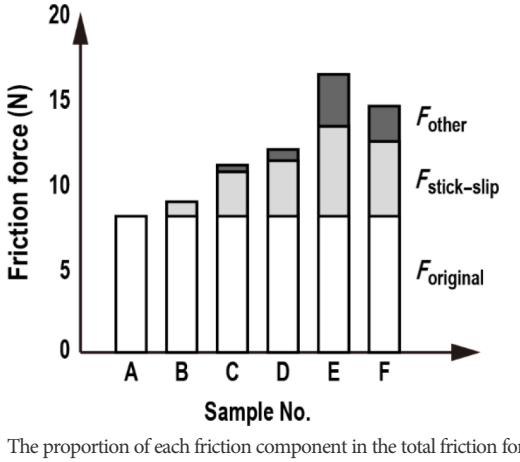


Fig. 12 The proportion of each friction component in the total friction force for each sample. $F_{original}$ denotes hysteresis friction force and adhesion friction force measured under non-hard particle sample; $F_{stick-slip}$ denotes friction force increase due to the proposed local stick–slip excitation; F_{other} denotes the amount of increase in adhesion friction force due to embedded particles or other effects.

introduces an internal stiffness distribution. Generally, the surface texture is considered useful for friction control. However, surface textures have a drawback in that their effects are lost when worn away. However, the benefit of introducing an internal stiffness distribution is that by applying multiple layers of stiffness distribution in the depth direction, even if the outermost stiffness layer is removed owing to wear, an underlying stiffness distribution layer will emerge, allowing the friction control effect to persist. Recent advancements in manufacturing technologies, such as the use of 3D printers for soft material production, have made it possible to create 3D structures and impart stiffness heterogeneity. By combining these technological developments with the findings of this study, we expect to realize innovative friction-control techniques.

5 Conclusions

In this paper, we present a novel friction control method that embeds hard particles within a soft material matrix to introduce internal stiffness inhomogeneity. This approach effectively leverages the interlocking effect between the embedded particles and surface asperities, which induces local stick–slip motion, resulting in increased macroscopic friction. Through experimental analysis, we demonstrated that the number density of hard particles and the corresponding elastic instability significantly influenced frictional performance. It is expected to also depend on the roughness of the counter surface, but it has been shown that an increase in friction force by about several tens of percent is possible, for example. These findings suggest that frictional force can be controlled and enhanced by optimizing the internal stiffness distribution of soft materials, offering a promising solution for applications requiring precise friction control.

The proposed method is unique to soft materials because it capitalizes on the energy dissipation caused by local stick–slip phenomena, a mechanism that is not observed in harder, more rigid materials. Future work could explore the scaling of this method to different soft material systems and investigate its potential for integration with advanced manufacturing techniques, such as 3D printing, to fabricate complex multilayered materials with graded stiffness properties.

Declaration of competing interest

The authors have no competing interests to declare that are relevant to the content of this article.

References

[1] Liu L W, Li K W, Lee Y H, Chen C C, Chen C Y. Friction measurements on “anti-slip” floors under shoe sole, contamination, and inclination conditions. *Safety Sci* **48**(10): 1321–1326 (2010)

[2] Yamaguchi T, Katsurashima Y, Hokkirigawa K. Effect of rubber block height and orientation on the coefficients of friction against smooth steel surface lubricated with glycerol solution. *Tribol Int* **110**: 96–102 (2017)

[3] Lorenz B, Persson B J, Fortunato G, Giustiniano M, Baldoni F. Rubber friction for tire tread compound on road surfaces. *J Phys: Condens Matter* **25**(9): 095007 (2013)

[4] Roberge J P, Ruotolo W, Duchaine V, Cutkosky M. Improving industrial grippers with adhesion-controlled friction. *IEEE Robot Autom Lett* **3**(2): 1041–1048 (2018)

[5] Persson B N J, Lorenz B, Shimizu M, Koishi M. Multiscale contact mechanics with application to seals and rubber friction on dry and lubricated surfaces. In: *Designing of Elastomer Nanocomposites: From Theory to Applications*. Stöckelhuber K W, Das A, Klüppel M, Eds. Cham: Springer, 2016: 103–156.

[6] Maegawa S, Itoigawa F, Nakamura T. A role of friction-induced torque in sliding friction of rubber materials. *Tribol Int* **93**: 182–189 (2016)

[7] Maegawa S, Itoigawa F, Nakamura T. Effect of surface grooves on kinetic friction of a rubber slider. *Tribol Int* **102**: 326–332 (2016)

[8] Bongaerts J H H, Fourtouni K, Stokes J R. Soft-tribology: Lubrication in a compliant PDMS–PDMS contact. *Tribol Int* **40**(10-12): 1531–1542 (2007)

[9] Murarash B, Itovich Y, Varenberg M. Tuning elastomer friction by hexagonal surface patterning. *Soft Matter* **7**(12): 5553 (2011)

[10] Mengüç Y, Sitti M. Gecko-inspired polymer adhesives. *Polym Adhes Frict Lubr*: 351–389 (2013)

[11] Sahli R, Pallares G, Ducottet C, Ben Ali I E, Al Akhrass S, Guibert M, Scheibert J. Evolution of real contact area under shear and the value of static friction of soft materials. *P Natl Acad Sci USA* **115**(3): 471–476 (2018)

[12] Kligerman Y, Varenberg M. Elimination of stick–slip motion in sliding of split or rough surface. *Tribol Lett* **53**(2): 395–399 (2014)

[13] Maegawa S, Itoigawa F, Nakamura T. Effects of stress distribution at the contact interface on static friction force: Numerical simulation and model experiment. *Tribol Lett* **62**(2): 15 (2016)

[14] Maegawa S, Itoigawa F, Nakamura T. New insight into the mechanism of static friction: A theoretical prediction of the effect of loading history on static friction force based on the static friction model proposed by Lorenz and Persson. *Tribol Int* **102**: 532–539 (2016)

[15] Tramsen H T, Gorb S N, Zhang H, Manoonpong P, Dai Z D, Heepe L. Inversion of friction anisotropy in a bio-inspired asymmetrically structured surface. *J R Soc Interface* **15**(138): 20170629 (2018)

[16] Aymard A, Delplanque E, Dalmas D, Scheibert J. Designing metainterfaces with specified friction laws. *Science* **383**(6679): 200–204 (2024)

[17] Piccardo M, Chateauminois A, Fretigny C, Pugno N M, Sitti M. Contact compliance effects in the frictional response of bioinspired fibrillar adhesives. *J R Soc Interface* **10**(83): 20130182 (2013)

[18] Cho Y, Kim G, Cho Y, Lee S Y, Minsky H, Turner K T, Gianola D S, Yang S. Orthogonal control of stability and tunable dry adhesion by tailoring the shape of tapered nanopillar arrays. *Adv Mater* **27**(47): 7788–7793 (2015)

[19] Moyle N, Dong H, Wu H B, Khripin C Y, Hui C Y, Jagota A. Increased sliding friction of a lubricated soft solid using an embedded structure. *Tribol Lett* **70**(1): 2 (2021)

[20] Moyle N, Wu H B, Khripin C, Bremond F, Hui C Y, Jagota A. Enhancement of elastohydrodynamic friction by elastic hysteresis in a periodic structure. *Soft Matter* **16**(6): 1627–1635 (2020)

[21] Ohzono T, Teraoka K. Unique load dependency of static friction of wrinkles formed on textile-embedded elastomer surfaces. *AIP Adv* **7**(5): 055309 (2017)

[22] Kılıç K İ, Temizer İ. Tuning macroscopic sliding friction at soft contact interfaces: Interaction of bulk and surface heterogeneities. *Tribol Int* **104**: 83–97 (2016)

[23] Tabor D. Hysteresis losses in the friction of lubricated rubber. *Rubber Chem Technol* **33**(1): 142–150 (1960)

[24] Roberts A D, Thomas A G. The adhesion and friction of smooth rubber surfaces. *Wear* **33**(1): 45–64 (1975)

[25] Roberts A D. A guide to estimating the friction of rubber. *Rubber Chem Technol* **65**(3): 673–686 (1992).

[26] Gabriel P, Thomas A G, Busfield J J C. Influence of interface geometry on rubber friction. *Wear* **268**(5–6): 747–750 (2010)

[27] Leroux J, Fulleringer B, Nélias D. Contact analysis in presence of spherical inhomogeneities within a half-space. *Int J Solids Struct* **47** (22–23): 3034–3049 (2010)

[28] Popov V L, Gray J A T. Prandtl-Tomlinson model: History and applications in friction, plasticity, and nanotechnologies. *Zamm-Z Angew Math Me* **92**(9): 683–708 (2012)

[29] Popov V L. The Prandtl-Tomlinson model for dry friction. In: *Contact Mechanics and Friction*. Berlin: Springer, 2010: 155–174.

[30] Maegawa S, Nakano K. Mechanism of stick–slip associated with Schallamach waves. *Wear* **268**(7–8): 924–930 (2010)

[31] Maegawa S, Itoigawa F, Nakamura T. Dynamics in sliding friction of soft adhesive elastomer: Schallamach waves as a stress-relaxation mechanism. *Tribol Int* **96**: 23–30 (2016)

[32] Fukahori Y, Yamazaki H. Mechanism of rubber abrasion. Part I: Abrasion pattern formation in natural rubber vulcanizate. *Wear* **171** (1–2): 195–202 (1994)

[33] Nakano K, Maegawa S. Stick–slip in sliding systems with tangential contact compliance. *Tribol Int* **42**(11–12): 1771–1780 (2009)



Kazushi Ito received his master degree in mechanical engineering in 2025 from Nagoya Institute of Technology, Aichi, Japan. After that, he enrolled in the doctoral program in engineering at Nagoya Institute of Technology.



Izumi Yoshida received his bachelor degree in mechanical engineering in 2022 from Nagoya Institute of Technology, Aichi, Japan. After that, he started his career as an engineer at Nakajima Planning where he participated in the Super Formula and SUPER GT championships. He is currently working at TOM'S Inc., Japan.



Xiaoxu Liu received her Ph.D. degree in mechanical engineering from Nagoya University, Japan, in 2018. Her current position is an assistant professor at Department of Electrical and Mechanical Engineering, Nagoya Institute of Technology, Japan. Her research area covers tribology of carbon-based coatings, precision micromachining using short-pulse laser, and laser surface modification.



Satoru Maegawa received his Ph.D. degree in mechanical engineering from Yokohama National University, Japan, in 2012. His current position is an associate professor at Department of Electrical and Mechanical Engineering, Nagoya Institute of Technology, Japan. His research area covers the tribology of soft materials, the control of friction-induced vibration, and laser-manufacturing technologies.



Fumihiro Itoigawa received his Ph.D. degree in mechanical engineering from Nagoya Institute of Technology, Japan. He has working experience at Nippondenso Co., Ltd., Japan, and University of Leeds, UK. His current position is a professor at the Department of Electrical and Mechanical Engineering, Nagoya Institute of Technology, Japan. His research areas are mechanical engineering, tribology, electronic engineering, design engineering, and surface engineering.



Naoya Amino is the head of Materials Performance Laboratory in the Yokohama Rubber Co., Ltd. (YRC), Japan. In 1993 he graduated from the Faculty of Engineering, Department of Polymer Chemistry, Kyoto University, Japan. Then he entered the Yokohama Rubber Co., Ltd., Japan. From 1998 he studied on friction mechanisms of silica filled- and carbon black filled-rubbers in Kanazawa University, Japan. Then he obtained his doctoral degree in 2001. He is researching and developing new rubber compounding technologies.